J. Fluid Mech. (2004), *vol.* 513, *pp.* 221–237.
DOI: 10.1017/S002211200400984X Printed in the United Kingdom

Universality and imaginary potentials in advection–diffusion equations in closed flows

By M. GIONA, S. CERBELLI AND V. VITACOLONNA

Dipartimento di Ingegneria Chimica, Università di Roma "La Sapienza", via Eudossiana 18, 00184 Roma

(Received 21 October 2003 and in revised form 19 January 2004)

This article addresses the scaling and spectral properties of the advection–diffusion equation in closed two-dimensional steady flows. We show that homogenization dynamics in simple model flows is equivalent to a Schrödinger eigenvalue problem in the presence of an imaginary potential. Several properties follow from this formulation: spectral invariance, eigenfunction localization, and a universal scaling of the dominant eigenvalue with respect to the Péclet number Pe. The latter property means that, in the high-Pe range (in practice $Pe \geqslant 10^2$–10^3), the scaling exponent controlling the behaviour of the dominant eigenvalue with the Péclet number depends on the local behaviour of the potential near the critical points (local maxima/minima). A kinematic interpretation of this result is also addressed.

1. Introduction

Dispersion of passive tracers is a central problem in fluid dynamics with practical implications for environmental sciences (pollutant dispersion), chemical reaction engineering (mixing), and more generally in all processes involving moving fluid phases.

Given a velocity field $\boldsymbol{v}(\boldsymbol{x}, t)$, dispersion problems are described by the second-order advection–diffusion equation (ADE)

$$\frac{\partial \phi}{\partial t} = -\nabla \cdot (\boldsymbol{v}\phi) + \varepsilon \nabla^2 \phi = \mathscr{L}[\phi], \tag{1.1}$$

where $\phi(\boldsymbol{x}, t)$ is the concentration field, and $\varepsilon = Pe^{-1}$ is the reciprocal of the Péclet number.

The study of (1.1) in fluid dynamics is aimed at determining how the structure and the qualitative properties of a velocity field determine and modify the dispersion dynamics (Batchelor 1956). In unbounded flows, the class that has been most investigated (see Childress & Soward 1989; Fannjiang & Papanicolau 1994; Majda & Kramer 1999 and references therein), the dispersion features are associated with statistical indicators (such as the mean square displacement) which are grounded on the equivalence between (1.1) and a stochastic Langevin equation (Castiglione *et al.* 1999). Most studies consider infinitely extended periodic flows (cellular flows), and the hypothesis that the flow domain is infinitely extended makes it possible to describe the asymptotic (long-distance and long-time) properties of (1.1) by means of a pure diffusion equation with constant tensor diffusivity (referred to as the *effective diffusivity*), by applying homogenization and perturbation techniques (Bensoussan, Lions & Papanicolau 1978; Majda & Kramer 1999). Consequently, the basic quantity for approaching mixing and dispersion in open unbounded flows is

the effective diffusivity, meaning that different dispersion regimes can be identified by considering the scaling of the effective diffusivity with the Péclet number. In particular, Fannjiang & Papanicolau (1994) found different dispersion regimes in two-dimensional autonomous flows, such as the *convection-enhanced regime*, for which the effective diffusivity is proportional to the square root of the Péclet number. The physical interpretation of the coupling between advection and diffusion in open flows, which leads to a nonlinear dependence of the effective diffusivity on the diffusion coefficient, is connected to the presence of channels and stagnation regions, which can be detected through the structure of the streamfunction (in two-dimensional flows or in three-dimensional simple flows), see e.g. Childress & Soward (1989).

In this article, a different class of flows is investigated, namely closed flows, i.e. flows in bounded domains, which is the natural physical setting for approaching mixing in batch stirred equipment and for analysing how stretching and folding mechanisms cope with diffusion in order to determine homogenization. The analysis of this problem has been carried out using the direct numerical simulation of (1.1) (Toussaint Carriere & Raynal 1995; Toussaint *et al.* 2000; Giona, Cerbelli & Adrover 2002; Cerbelli, Adrover & Giona 2003) and different scaling regimes have been observed, depending on whether the velocity field gives rise to non-chaotic, partially or globally chaotic Lagrangian kinematics (Ottino 1989). For closed and bounded flows, the concept of dispersion regimes is properly addressed within a spectral characterization of the advection–diffusion operator (or the Poincaré operator associated with it in time-periodic flow fields) (see Giona *et al.* 2002), in terms of the scaling of the eigenvalue spectrum vs the Péclet number (Cerbelli *et al.* 2003).

The aim of this article is to propose a new approach to dispersion phenomena in bounded two-dimensional autonomous flows. This approach is based on the concept of imaginary potentials (see § 3.1) which allows an interpretation of all the salient features of dispersion in a simple and rigorous way. Specifically, we show that the advection–diffusion equation in simple two-dimensional flows possesses universal features, and this phenomenon has a one-to-one correspondence with the localization properties of the eigenfunctions. The results obtained can be generalized to interpret more complex flows.

2. Homogenization in closed flows

As outlined in the Introduction, the interaction between advection and diffusion has been theoretically investigated mainly in the case where the scalar field evolves in an infinitely extended space, i.e. $\mathscr{R}^2$ or $\mathscr{R}^3$, in the presence of a spatially periodic flow generated by the repetition along the coordinate axes of a unit flow cell structure (*cellular flow*). While it is beyond the aim of this article to provide an overview of results and techniques used to approach advection–diffusion in unbounded flows (a comprehensive review of methods and results can be found in Majda & Kramer 1999), it is nevertheless useful to stress the physical setting of the problem, in order to highlight to what extent it is different from the homogenization dynamics of an advecting–diffusing scalar field that evolves in a closed bounded domain.

When investigating advection–diffusion in a cellular flow (with vanishing average velocity), the focus is to determine how the flow structure impacts upon the dynamics of a scalar concentration field initially localized onto a bounded set (e.g. in the limit, the dynamics of a Dirac's δ-distribution). By envisioning the advection–diffusion equation as the Fokker–Plank formulation of the corresponding Langevin equation of particle kinematics, a first quantitative characterization of dispersion is to determine

how the size of a cloud of tracers, initially localized in the given bounded region, depends on time in the asymptotic limit. The main physical observation that motivates the analytical developments is that, given long enough time, the characteristic lengthscale defining the 'size of the cloud' will be very much larger than the one defining the scale of spatial flow variation (i.e. the length of the unit cell).

Thus, dispersion phenomena in unbounded domains described by (1.1) prove equivalent (the proper mathematical setting of this equivalence is addressed in Bensoussan *et al.* 1978; Majda & Kramer 1999) to an anisotropic diffusion process, characterized by a constant tensor diffusivity (*effective diffusivity tensor*) $\mathscr{D}^*$, which is a constant 'bulk property' of the flow when the convection process is observed at such a macroscopic scale. The Lagrangian interpretation of this result is that the structure of any initial swarm of particles will asymptotically approach an ellipsoid, whose principal axes, say d_i ($i = 1, n$, $n = 2, 3$) scale with time according to $d_i \sim \sqrt{2D_i t}$ where D_i are the eigenvalues of $\mathscr{D}^*$, which, since $\mathscr{D}^*$ is symmetric and positive definite, are real and positive.

From these observations, it is clear that a quantitative characterization alternative to that used for unbounded flows must be sought if one is to describe the advection–diffusion process in a closed bounded flow, i.e. where the flow domain is a bounded manifold $\mathscr{M}$, characterized by a finite lengthscale (diameter). Two subcases can be considered, according to whether the manifold possesses a non-empty boundary (e.g. $\mathscr{M}$ is a given region of R^n, $n = 2, 3$, delimited by a closed surface), or $\mathscr{M}$ is a boundaryless manifold (e.g. the two-torus, the three-torus, the surface of a sphere, and so on). In the case where $\mathscr{M}$ possesses a non-empty boundary, say $\partial\mathscr{M}$, by the term *closed flow* we mean the physical setting specified by the following two conditions: (i) the boundary is impermeable to the flow, i.e. $\boldsymbol{v}\cdot\boldsymbol{n} = 0$ on $\partial\mathscr{M}$, $\boldsymbol{n}$ being the unit vector normal to the boundary at any given point of $\partial\mathscr{M}$, and (ii) the diffusive flux of passive scalar ϕ through $\partial\mathscr{M}$ vanishes. This implies that the overall flux through the boundary also vanishes and, consequently, the integral of the concentration field over the bounded domain $\mathscr{M}$ is conserved. Bounded closed flows are particularly important in theoretical and applied fluid dynamics, since they represent realistic models of laboratory flows (driven cavity, flow between concentric/eccentric cylinders, etc.) and of engineering applications (closed stirred vessel), see e.g. Ottino (1989). Moreover, they provide the most convenient setting for studying the global properties of advection, associated with the folding of material lines and surface elements, and with the occurrence of Lagrangian chaos (Ottino 1989).

Restricting our focus to autonomous deterministic flows, it turns out that spectral theory provides the key tool for approaching homogenization dynamics in bounded closed flows. Indeed, it has been proved that, under fairly general conditions on the velocity field $\boldsymbol{v}$, the advection–diffusion operator $\mathscr{L}$ possesses a pure point spectrum composed of (possibly complex) separated eigenvalues $\lambda_n = -\lambda_n^R + \mathrm{i}\theta_n$ ($\lambda_n^R \geqslant 0$), $n = 0, 1, \ldots$, and the corresponding eigenfunctions form a basis for the functional space of square summable functions that satisfy the proper set of boundary conditions expressing the closed structure of the flow (Agmon 1962, 1965). In passing, we note that the spectrum of $\mathscr{L}$ in the unbounded case may be continuous. The reciprocal of the real parts of the eigenvalues define the time constants $\tau_n = 1/\lambda_n^R$ associated with the exponential decay characterizing each of the invariant subspaces spanned by the eigenfunctions. The worst possible (i.e. slowest) case is represented by the eigenvalue possessing the real part with the smallest modulus. Given a generic initial condition, it is this timescale that will define the asymptotic dynamics of homogenization starting from a generic initial distribution. Therefore, the first quantitative characterization

of mixing in bounded closed autonomous flows is to determine how the eigenvalues scales with Pe and depend upon the structure of the velocity field.

3. Statement of the problem

Consider the ADE for a scalar concentration field defined on the two-dimensional torus (i.e. on the unit square $\mathscr{I}^2 = \{(x, y) \mid 0 \leqslant x, y \leqslant 1\}$) with opposite edges identified) for a simple velocity field: $\boldsymbol{v}(\boldsymbol{x}) = (0, \sin(2\pi x))$, where $\boldsymbol{x} = (x, y)$. This model is referred to as the autonomous sine flow (ASF) and has been widely investigated (Liu, Muzzio & Peskin 1994; Giona & Adrover 1998). For ASF, the advection–diffusion operator becomes

$$\mathscr{L}[\phi] = -\sin(2\pi x)\frac{\partial \phi}{\partial y} + \varepsilon\left(\frac{\partial^2 \phi}{\partial x^2} + \frac{\partial^2 \phi}{\partial y^2}\right), \tag{3.1}$$

with the boundary conditions

$$\left.\begin{aligned} \phi(x, 0, t) = \phi(x, 1, t), \qquad & \left.\frac{\partial \phi(x, y, t)}{\partial y}\right|_{y=0} = \left.\frac{\partial \phi(x, y, t)}{\partial y}\right|_{y=1}, \\ \phi(0, y, t) = \phi(1, y, t), \qquad & \left.\frac{\partial \phi(x, y, t)}{\partial x}\right|_{x=0} = \left.\frac{\partial \phi(x, y, t)}{\partial x}\right|_{x=1}, \end{aligned}\right\} \tag{3.2}$$

and with the initial condition $\phi(\boldsymbol{x}, t)|_{t=0} = \phi_0(\boldsymbol{x})$. The boundary value problem defined by (3.1) and by the periodic boundary conditions (3.2) is equivalent to a problem defined on the two-dimensional torus (which is a boundaryless manifold) in that periodic boundary conditions on the scalar field and the periodicity of the advecting flow field imply that the net flux of the scalar field leaving the unit square at any point of the boundary re-enters the system at the corresponding point on the opposite edge.

Despite its formal simplicity, the ASF is a valid and interesting prototypical model flow for addressing the coupling between advection and diffusion in two-dimensional autonomous flows in closed domains (Giona *et al.* 2002).

For closed and bounded flows, a complete characterization of homogenization dynamics generated by the operator $\mathscr{L}$ can be achieved through its spectral (eigenvalue/eigenfunction) properties. The most relevant quantity is the dominant eigenvalue (and the corresponding eigenfunction), that is, the eigenvalue possessing the largest real part. The dominant eigenvalue defines, for generic initial conditions, the slowest timescale of relaxation toward the equilibrium condition which corresponds to the constant profile $\phi_{\mathrm{eq}}(\boldsymbol{x})$ uniform throughout the flow domain (by mass conservation this is equal to the mean value of the initial concentration $\phi_0(\boldsymbol{x})$).

The salient spectral feature of the sine flow (which is shared by two-dimensional autonomous flows in closed domains, such as, e.g., the driven cavity flow) is the occurrence of two eigenvalue branches (Giona *et al.* 2002; Cerbelli *et al.* 2003): (i) a diffusive branch, the eigenvalues $\{\lambda_n\}$ of which scale linearly with ε, $\lambda_{n,\mathrm{dif}} \sim \varepsilon$, and (ii) a convective branch, the eigenvalues of which scale as $\lambda_{n,\mathrm{con}} \sim \sqrt{\varepsilon}$. The latter branch qualitatively possesses the same scaling behaviour as observed in unbounded cellular flows (Fannjiang & Papanicolau 1994), and referred to as convection-enhanced diffusion.

3.1. *Homogenization and imaginary potentials*

The occurrence of two different spectral branches, as well as other properties of the advection–diffusion equation, can be explained by introducing the following

representation:

$$\phi(x, y) = \mathrm{e}^{-\mathrm{i}2\pi m y}\psi(x), \tag{3.3}$$

where m is an integer, and $\mathrm{i} = \sqrt{-1}$. By substituting (3.3) into (3.1), the ADE splits into a countable family of one-dimensional problems associated with the operators:

$$\mathscr{L}[\psi](x) = \varepsilon\frac{\mathrm{d}^2\psi(x)}{\mathrm{d}x^2} - 4\pi m^2\varepsilon\psi(x) + \mathrm{i}2\pi m\sin(2\pi x)\psi(x). \tag{3.4}$$

For $m = 0$, the eigenvalues of $\mathscr{L}$ scale diffusively, while for $m \neq 0$ an effective coupling between advection and diffusion takes place. This leads to a non-trivial dependence of the eigenvalues upon ε.

Equation (3.4) indicates that $\mathscr{L}[\phi]$ is the linear combination of two operators: a diagonal operator $-4\pi m^2\varepsilon\psi$, and the second-order complex-valued operator $\mathscr{A}[\psi]$, defined by

$$\mathscr{A}[\psi](x) = \varepsilon\frac{\mathrm{d}^2\psi(x)}{\mathrm{d}x^2} + \mathrm{i}V_m(x)\psi(x), \tag{3.5}$$

where $V_m(x) = 2\pi m\sin(2\pi x)$. The operator $\mathscr{A}$ can be viewed as a Schrödinger operator in the presence of an imaginary potential $\mathrm{i}V_m(x)$ defined on the unit circumference (i.e. on the unit interval $]0, 1[$ with periodic boundary condition). In fact, the imaginary nature of the potential implies that $\mathscr{A}$ is a dissipative operator (see below). For this reason, we will use the wording 'family of potentials associated with a velocity field' to indicate the relationship between $V_m(x)$, and $\boldsymbol{v}(\boldsymbol{x})$, and this should not be confused with the concept of velocity potential of classical fluid dynamics.

Without loss of generality, we consider the case $m = 1$, dropping the subscript m, i.e. defining $V(x) = V_1(x)$ (this is sensible, as the dominant eigenfunction of $\mathscr{L}$ is obtained for $m = 1$).

3.2. *Functional relations for the eigenvalues*

Some significant properties of the advection–diffusion operator can be obtained by investigating the functional-theoretical properties of the operator $\mathscr{A}$ defined by (3.5). Let us first introduce some basic notation. The eigenfunctions of $\mathscr{A}$ are complex-valued functions belonging to the functional space $L^2_{\mathrm{per}}(]0, 1[)$ of square summable periodic functions in the interval $]0, 1[$. The functional space $L^2_{\mathrm{per}}(]0, 1[)$ is a Hilbert space which has the inner product

$$(f, g) = \int_0^1 f(x)\overline{g}(x)\,\mathrm{d}x, \qquad f, g \in L^2_{\mathrm{per}}(]0, 1[), \tag{3.6}$$

where $\overline{g}(x)$ is the complex conjugate of $g(x)$. The natural L^2-norm is induced by the inner product (3.6): $\|f\|_{L^2} = (f, f)^{1/2}$.

Let $\mu = \mu_R + \mathrm{i}\omega$ be an eigenvalue of $\mathscr{A}$, and ψ the corresponding eigenfunction:

$$\varepsilon\frac{\mathrm{d}^2\psi(x)}{\mathrm{d}x^2} + \mathrm{i}V(x)\psi(x) = \mu\psi(x). \tag{3.7}$$

Multiplying (3.7) by $\overline{\psi}(x)$, and integrating over $]0, 1[$, it follows that

$$-\varepsilon\|\mathrm{D}\psi\|^2_{L^2} + \mathrm{i}(V\psi, \psi) = \mu\|\psi\|_{L^2}, \tag{3.8}$$

where $\mathrm{D}\psi(x) = \mathrm{d}\psi(x)/\mathrm{d}x$, i.e.

$$\mu_R = -\frac{\varepsilon\|\mathrm{D}\psi\|^2_{L^2}}{\|\psi\|^2_{L^2}}, \qquad \omega = \frac{(V\psi, \psi)}{\|\psi\|^2_{L^2}}. \tag{3.9}$$

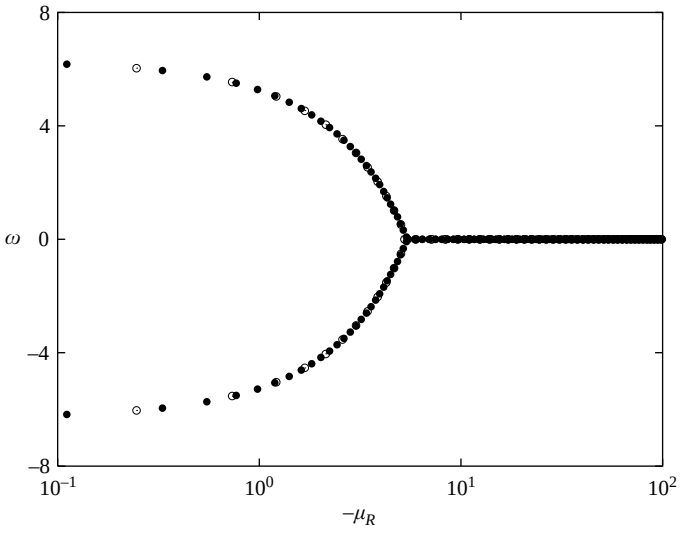

FIGURE 1. Spectrum of the operator $\mathscr{A}$: ○, $\varepsilon = 10^{-3}$; ●, $\varepsilon = 2 \times 10^{-4}$.

Since $\psi(x) =$ constant is not an eigenfunction for $\mathscr{A}$ unless $V(x) =$ constant, this expression for μ_R indicates that the eigenvalues of $\mathscr{A}$ possess a strictly negative real part that ensures dissipativity.

Another useful expression for the eigenvalues of $\mathscr{A}$ follows by integrating (3.7) over]0, 1[. By enforcing periodicity, the integral of $\mathrm{d}^2\psi(x)/\mathrm{d}x^2$ vanishes; thus one obtains

$$\mu \int_0^1 \psi(x)\,\mathrm{d}x = \mathrm{i} \int_0^1 V(x)\psi(x)\,\mathrm{d}x, \tag{3.10}$$

which can be expressed as $\mu(\psi, 1) = \mathrm{i}(\psi, V)$.

4. Universality in the eigenvalue scaling

4.1. *Spectral invariance and localization*

The eigenvalue spectrum of the operator $\mathscr{A}$ for $V(x) = 2\pi \sin(2\pi x)$ is depicted in figure 1 for different values of ε. The spectrum possesses a fork-like shape corresponding to the presence of both complex (forming the two arms of the fork) and purely real eigenvalues. One observes that the slowest decaying eigenvalues are complex-valued.

Spectral invariance characterizes the eigenvalue distribution of $\mathscr{A}$: at small ε values the eigenvalues are located on a invariant set as depicted in figure 1. This phenomenon has been observed by Hatano & Nelson 1996 in the study of the non-Hermitian Schrödinger equation in the presence of an imaginary vector potential (corresponding to the action on a quantum particle of a magnetic field) superimposed on a random potential (see further Goldsheid & Khoruzhenko 2000).

In order to characterize the dispersion properties of the ADE, the most important spectral feature of the operator $\mathscr{A}$ is the localization of the eigenfunctions belonging to the complex-conjugate arms of the spectrum. Figure 2(*a*) depicts the modulus $|\psi(x)|$ of the dominant eigenfunction for several values of the Péclet number, and shows that the eigenfunctions are strongly localized around the critical point $x_c = 1/4$ of the potential. In fact, the dominant eigenfunctions $\psi_\varepsilon(x)$ for different $\varepsilon \to 0$ can

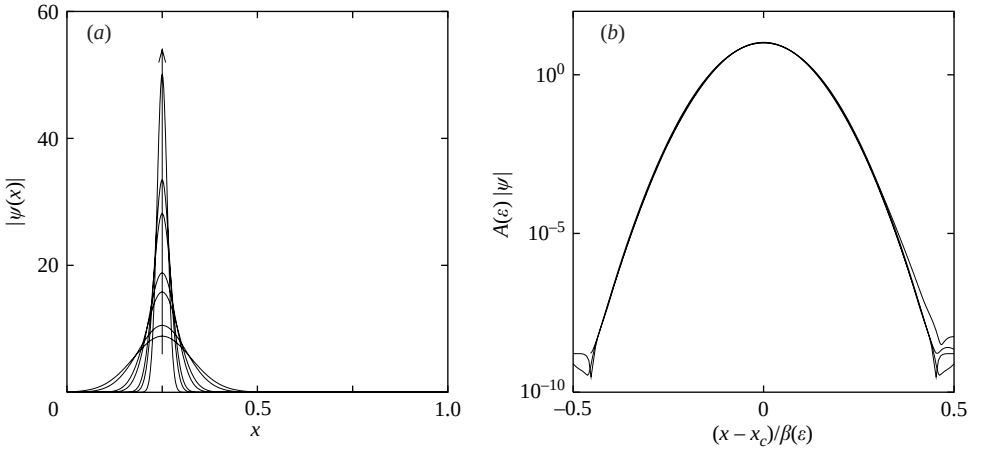

FIGURE 2. Dominant eigenfunction of the operator $\mathscr{A}$ for different values of the Péclet number ($\varepsilon = Pe^{-1}$). (*a*) $|\psi(x)|$ vs x. The arrow indicates increasing values of Pe, $Pe = 5\times10^2, 10^3, 5\times10^3, 10^4, 5\times10^4, 10^5, 5\times10^5$. (*b*) Validity of (4.1) for rescaling the eigenfunction: $A(\varepsilon)|\psi|$ vs $(x-x_c)/\beta(\varepsilon)$, for $Pe = 10^3, 10^4, 10^5, 10^6$.

be rescaled into a single master curve $g(\xi)$ (see figure 2*b*):

$$\psi_\varepsilon(x) = A^{-1}(\varepsilon) g(\xi)|_{\xi=(x-x_c)/\beta(\varepsilon)} \tag{4.1}$$

where $A(\varepsilon)$ is a normalization constant, and the scaling function $\beta(\varepsilon) > 0$ is proportional to $\varepsilon^{1/4}$ (see § 4.2 for a theoretical justification of this result).

The eigenfunctions depicted in figure 2 are normalized so that $(\psi_R, 1) = (\psi_I, 1) = 1$, where $\psi_R(x)$ and $\psi_I(x)$ are the real and the imaginary part of $\psi(x)$, respectively, and $|\psi(x)| = \sqrt{\psi_R^2(x) + \psi_I^2(x)}$. The rescaling of the eigenfunction into a single master curve has been obtained by setting $A(\varepsilon) = \beta(\varepsilon)$. A similar behaviour occurs for the other eigenfunctions of the spectrum associated with complex eigenvalues.

4.2. *Universality*

The localization property of the eigenfunctions for the second-order operator $\mathscr{A}$ in the presence of an imaginary potential is the indicator of a universal scaling characterizing the advection–diffusion equation. In order to address this issue, let us first consider a particular class of periodic potentials defined by the properties that: (i) $V(x)$ possesses a single local maximum at $x = 0$, and a single local minimum at $x = x_m > 0$, such that $V(0) = -V(x_m)$, and that (ii) $V(x)$ near $x = 0$ and $x = x_m$ attains the same nonlinear behaviour characterized by the same exponent γ:

$$\left.\begin{aligned} V(x) &= V_M - V_1|x|^\gamma + o(|x|^\gamma) && \text{for } |x| < \eta \\ V(x) &= -V_M + V_1|x-x_m|^\gamma + o(|x-x_m|^\gamma) && \text{for } |x-x_m| < \eta, \end{aligned}\right\} \tag{4.2}$$

where $\eta > 0$. For example the sine flow model falls into this class by considering the translation $x' = x - 1/4$, and is a quadratic potential, i.e. $\gamma = 2$. In the 'pathological' case of a potential $V(x)$ which possesses maxima and minima, in the neighbourhood of which $V(x)$ is constant (flat critical points), the value $\gamma = \infty$ can be assigned to these critical points, since $\gamma = \infty$ can be viewed as the limit value for the exponents γ_n $n = 1, 2, \ldots$ associated with an analytic sequences of potentials $V_n(x)$ converging to $V(x)$.

Since we are considering the behaviour of the eigenvalues and eigenfunctions as $\varepsilon \to 0$, we will indicate explicitly their dependence on ε when $\mu = \mu(\varepsilon)$ and $\psi = \psi_\varepsilon(x)$.

Let us assume (4.1), i.e. $\psi_\varepsilon(x) = A^{-1}(\varepsilon) g(x/\beta(\varepsilon))$. By substituting this expression into (3.7), and performing the change of variable $\xi = x/\beta(\varepsilon)$ it follows that

$$-\mu_R(\varepsilon) = \frac{\varepsilon}{\beta^2(\varepsilon)} \frac{\displaystyle\int_{-1/2\beta(\varepsilon)}^{1/2\beta(\varepsilon)} |\mathrm{D}g(\xi)|^2 \,\mathrm{d}\xi}{\displaystyle\int_{-1/2\beta(\varepsilon)}^{1/2\beta(\varepsilon)} |g(\xi)|^2 \,\mathrm{d}\xi}, \tag{4.3}$$

where $\mathrm{D}g(\xi) = \mathrm{d}g(\xi)/\mathrm{d}\xi$. Since the master function $g(\xi)$ is vanishingly small outside a narrow interval centred around $\xi = 0$ and since, for $\varepsilon \to 0$, the integration limits approach $\pm\infty$, (4.3) implies

$$-\mu_R(\varepsilon) \simeq C \frac{\varepsilon}{\beta^2(\varepsilon)}, \tag{4.4}$$

where $C = \int_{-\infty}^{\infty} |\mathrm{D}g(\xi)|^2 \,\mathrm{d}\xi / \int_{-\infty}^{\infty} |g(\xi)|^2 \,\mathrm{d}\xi$.

Let us now consider (3.10). By applying the scaling assumption for $\psi_\varepsilon(x)$, and by making the same approximation regarding the integration limits, one obtains

$$\mu \int_{-\infty}^{\infty} g(\xi) \,\mathrm{d}\xi = \mathrm{i} \int_{-\infty}^{\infty} V(\beta(\varepsilon)\xi) g(\xi) \,\mathrm{d}\xi. \tag{4.5}$$

Owing to the fact that $g(\xi)$ is localized around $\xi = 0$, the integral on the right-hand side of (4.5) depends on the local behaviour of $V(\beta(\varepsilon)\xi)$ near $\xi = 0$. Therefore we can apply the local expansion (4.2), thus obtaining a linear system for the two unknowns $\mu_R(\varepsilon)$ and $\omega(\varepsilon)$:

$$\begin{bmatrix} A_{0,R} & -A_{0,I} \\ A_{0,I} & A_{0,R} \end{bmatrix} \begin{bmatrix} \mu_R(\varepsilon) \\ \omega(\varepsilon) \end{bmatrix} = \begin{bmatrix} -V_M A_{0,I} + V_1 \beta^\gamma(\varepsilon) A_{1,I} \\ V_M A_{0,R} - V_1 \beta^\gamma(\varepsilon) A_{1,R} \end{bmatrix} \tag{4.6}$$

where

$$A_{0,k} = \int_{-\infty}^{\infty} g_k(\xi) \,\mathrm{d}\xi, \qquad A_{1,k} = \int_{-\infty}^{\infty} |\xi|^\gamma g_k(\xi) \,\mathrm{d}\xi, \qquad k = R, I, \tag{4.7}$$

and $g(\xi) = g_R(\xi) + \mathrm{i} g_I(\xi)$. The solution of the linear system (4.6) is

$$-\mu_R(\varepsilon) = \beta^\gamma(\varepsilon) \frac{V_1(A_{0,I}A_{1,R} - A_{0,R}A_{1,I})}{A_{0,R}^2 + A_{0,I}^2}, \tag{4.8}$$

$$\omega(\varepsilon) = V_M - \beta^\gamma(\varepsilon) \frac{V_1(A_{0,R}A_{1,R} + A_{0,I}A_{1,I})}{A_{0,R}^2 + A_{0,I}^2}. \tag{4.9}$$

Let us first consider the scaling behaviour of the real part of the eigenvalues with ε. By equating (4.4) and (4.8) it follows that

$$\beta(\varepsilon) = B\varepsilon^{1/(2+\gamma)}, \tag{4.10}$$

where B is a positive constant, and therefore from (4.4) one obtains

$$-\mu_R(\varepsilon) \sim \varepsilon^\alpha, \tag{4.11}$$

where the exponent α is given by

$$\alpha = \frac{\gamma}{2+\gamma}. \tag{4.12}$$

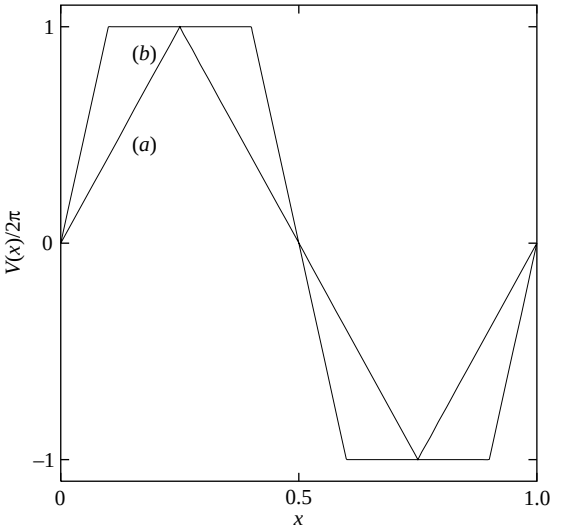

FIGURE 3. Potential $V(x)$ given by (4.13): (*a*) $h = 1/4$, (*b*) $h = 0.1$.

Equation (4.12) is the main result regarding universality, since it expresses the scaling behaviour of the dominant eigenvalue as a function of the local behaviour near the critical point. In the case of quadratic potentials (as for the sine-flow) $\gamma = 2$, and therefore $\alpha = 1/2$ as observed numerically. The formal analogy with the Feigenbaum universality (Feigenbaum 1979) for the period-doubling cascade of unimodular maps on the interval is evident, since in both cases the scaling exponents depend exclusively on the local behaviour near the critical point.

In order to assess further the validity of (4.12), let us consider a family of trapezoidal potentials (see figure 3):

$$V(x) = \begin{cases} 2\pi x/h, & x \in]0, h] \\ 2\pi, & x \in]h, 1/2 - h] \\ \pi(1 - 2x)/h, & x \in]1/2 - h, 1/2 + h] \\ -2\pi, & x \in]1/2 + h, 1 - h] \\ 2\pi(x - 1)/h, & x \in]1 - h, 1], \end{cases} \tag{4.13}$$

where $h \in [0, 1/4]$. For $h = 1/4$, $V(x)$ expressed by (4.13) yields a tent potential and therefore $\gamma = 1$. For $h \to 0$, $V(x)$ approaches a square-wave potential, and thus $\gamma = \infty$. For intermediate values of h, $V(x)$ yields a trapezoidal symmetric potential, which is flat near the critical point, and thus $\gamma = \infty$. Equation (4.12) predicts the value $\alpha = 1/3$ for $h = 1/4$, while for any other value of h within the interval $[0, 1/4[$, $\alpha = 1$, i.e. the dominant eigenfunction scales diffusively. These results are confirmed by numerical spectral simulations (obtained by applying a QR algorithm to the Galërkin representation of (3.7) expanded in the Fourier basis $\{e^{i2\pi nx}\}$). Figure 4 reviews the scaling behaviour of the dominant eigenvalue as a function of the Péclet number (ε is the reciprocal of Pe) for the class of symmetric potentials described above. Lines (*a*), (*b*) and (*c*) refer to the tent potential ((4.13) with $h = 1/4$), to the sine flow and to the square-wave potential ((4.13) for $h \to 0$), respectively. As predicted by (4.12) the value of the exponent α, $-\mu_R \sim Pe^{-\alpha}$, is in these three cases $\alpha = 1/3, 1/2$ and 1, respectively. The spectral behaviour in the presence of the potential (4.13) for $h \to 1/4^-$ merits particular interest. Figure 4 shows this case, curves (*d–f*)

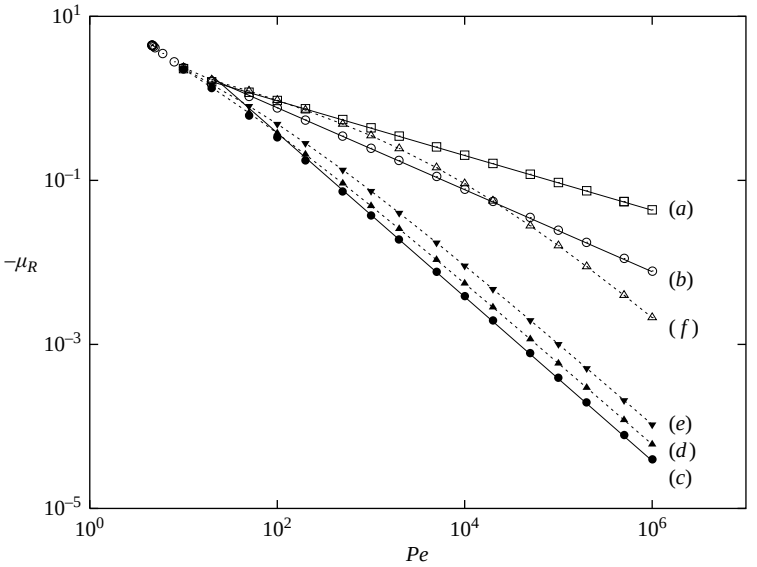

FIGURE 4. Dominant eigenvalue of $\mathscr{A}$ vs the Péclet number Pe. (a) Tent potential, (b) sine-flow potential, (c) square-wave potential. (d–f) The potential (4.13) for $h = 0.05, 0.10$ and 0.22, respectively. Solid lines (a–c) correspond to the theoretical exponent α as predicted by (4.12) i.e. to $\alpha = 1/3, 1/2, 1$ respectively. Dotted lines (d–f) are interpolating curves drawn for visualization purposes.

for $h = 0.05, 0.10$, and 0.22. The large-Péclet-number scaling is characterized by an exponent α equal to 1, in agreement with (4.12). Nevertheless, as h approaches the value $1/4$ from below, a crossover occurs in the behaviour of $-\mu_R$ (this is clearly evident from line (f) in figure 4): at low Péclet numbers the spectral scaling is similar to that of the tent potential, while the large-Péclet-number limit is dominated by the local behaviour near the critical point, thus resulting in an asymptotic diffusive scaling $-\mu_R \sim 1/Pe$.

Regarding the imaginary part of the eigenvalues, (4.9)–(4.10) indicate that $\omega(\varepsilon) = V_m - D\varepsilon^\alpha$, where D is a constant, and therefore $\lim_{\varepsilon \to 0^+} \omega(\varepsilon) = V_M$, i.e. at vanishingly small diffusivities, the imaginary part of the eigenvalues approaches the value of the potential at the critical point. This observation is confirmed by the numerical spectral results (see e.g. figure 1, showing that the dominant imaginary part converges to 2π for the ASF).

The results obtained for the simple model flows generated by a symmetric potential $V(x)$ can be extended to more complex situations. In the case of flows on the unit square (with periodic boundary conditions, still of the form $\boldsymbol{v}(\boldsymbol{x}) = (0, V(x)/2\pi)$, but with $V(x)$ generic smooth periodic function in $]0, 1[$, the dominant eigenfunction of $\mathscr{A}$ is still localized and, if all the critical points of $V(x)$ are quadratic, the dominant eigenvalue scales at large Pe as $-\mu_R \sim Pe^{-1/2}$. For example, figure 5(a) shows a multiscale potential $V(x)/2\pi = \sin(2\pi x) + 0.5\sin(4\pi x) + 0.25\sin(16\pi x)$, and figure 5($b$) the norm of the eigenfunctions for large Pe. This result can be further generalized to a generic vector potential $V(x)$: the asymptotic scaling (for $\varepsilon \to 0$) of the real part of the dominant eigenvalue is controlled by the largest value of the exponent γ at its critical points.

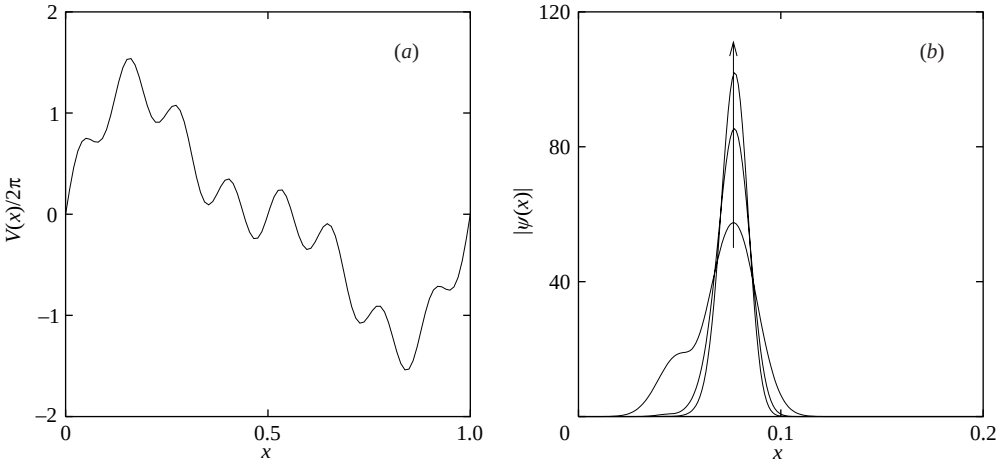

FIGURE 5. (*a*) Multiscale potential $V(x)$ (see main text). (*b*) Corresponding dominant eigenfunctions of $\mathscr{A}$. The arrow indicates increasing values of $Pe = 10^5, 5 \times 10^5, 10^6$.

It is important to observe that the method used for the estimate of the eigenvalue scaling is based on exact norm conditions (3.9)–(3.10) for the values attained by μ, and on the empirical assumption related to the eigenfunction localization (4.1). There is no perturbative approximation of the eigenfunctions, as e.g. in the Wentzel, Kramers and Brillouin (WKB) approximation of second-order eigenvalue problems (Holmes 1995).

4.3. *Monotonic potentials*

The theory developed in § 4.2 indicates that shear flows on the two-dimensional torus driven by a continuous velocity field $\boldsymbol{v}(\boldsymbol{x}) = (0, v(x))$ yield generically a value of the exponent $\alpha = 1/2$. Deviations from this scaling behaviour may occur (as e.g. for the class of potentials (4.12)), but these cases represent paradigmatic model flows, interesting for theoretical analysis, but of marginal practical relevance.

There is, however, an important and practically relevant case that deserves discussion, namely the class of potentials $V(x)$ which are non-uniform but monotonic for $x \in (0, 1)$. These model flows can be used, e.g., to predict the homogenization properties of laminar Couette flows.

The class of monotonic flows in $\mathscr{I}^2$ is very peculiar since, due to the periodicity of the flow domain (the unit square $\mathscr{I}^2$ with periodic boundary conditions), the potential $V(x)$ is no longer continuous at the edges, i.e. $V(0) \neq V(1)$. As a prototypical model, consider the potential given by

$$V(x) = 4\pi(x - 1/2). \tag{4.14}$$

Figure 6(*a*) shows the behaviour of the dominant eigenfunction for different values of the Péclet number. As expected, the dominant eigenfunction is localized next to the discontinuity (corresponding to $x = 1$). Moreover, the localization occurs solely at one side of the discontinuity. Owing to the symmetry of the potential $V(x) = -V(1 - x)$, for each complex eigenvalue/eigenfunction μ, $\psi(x)$, the function $\overline{\psi}(1 - x)$ is also an eigenfunction of $\mathscr{A}$ associated with the complex-conjugate eigenvalue $\overline{\mu}$. Therefore, there exist two different eigenfunctions associated with the dominant eigenvalues $-\mu^R \pm \mathrm{i}\omega$, with the smallest real part $-\mu^R$, each of which is localized either to the left or to the right of the discontinuity (due to periodicity of the flow domain $x = 0$

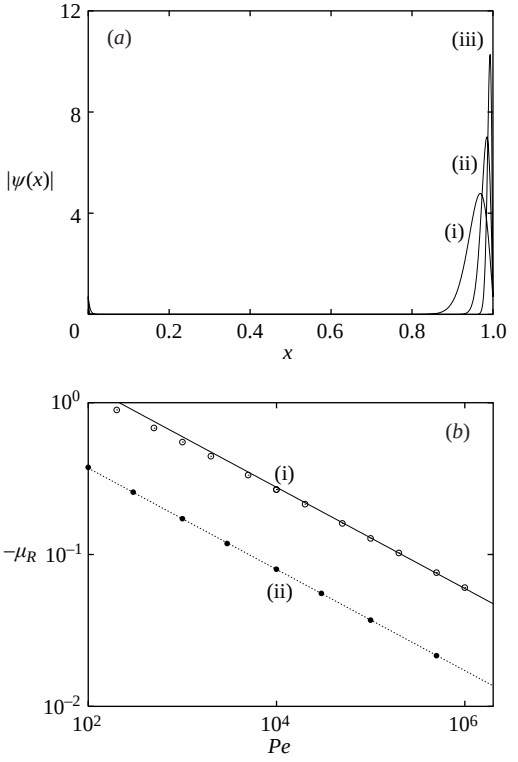

FIGURE 6. (*a*) Dominant eigenfunction for the discontinuous potential (4.14) $V(x) = 4\pi(x - 1/2)$. (i)–(iii) $Pe = 10^4, 10^5\ 10^6$, respectively. (*b*) Dominant eigenvalue $-\mu_R$ vs Pe. ○, The spectral results for the discontinuous potential (4.14). •, Direct numerical simulation results for the planar Couette flow. (i) and (ii) The theoretical scaling $-\mu_R \sim Pe^{-1/3}$.

and $x = 1$ coincide). Without loss of generality, let us assume that the potential $V(x)$ is continuous in any open set of $(0, 1)$, monotonically increasing and with a linear behaviour in the neighbourhood of the discontinuity located at $x = 0$.

In order to obtain the scaling of the dominant eigenvalue, we can readily follow the approach developed in § 4.2, by expanding the potential $V(x)$ in the neighbourhood of the discontinuity:

$$\left.\begin{aligned} V(x) &= V_0^- + V_1^- x, \qquad x < 0 \\ V(x) &= V_0^+ + V_1^+ x, \qquad x > 0 \end{aligned}\right\} \tag{4.15}$$

where $V_0^- \neq V_0^+$. Equation (4.4) holds true, but the application of (4.5) needs some manipulations. By enforcing the empirical observation that each eigenfunction is localized on a single side of the discontinuity, (4.5) is modified to

$$\mu \int_{-\infty}^{0} g(\xi)\,\mathrm{d}\xi = \mathrm{i} \int_{-\infty}^{0} V(\beta(\varepsilon)\xi) g(\xi)\,\mathrm{d}\xi, \tag{4.16}$$

where the case of eigenfunctions localized to the left of the discontinuity (as in figure 6*a*) is considered. By substituting the local expansion (4.15) into (4.16) and solving the resulting linear system, one finally obtains

$$-\mu_R(\varepsilon) = \beta(\varepsilon) \frac{V_1^- (A_{0,I}^- A_{1,R}^- - A_{0,R}^- A_{1,I}^-)}{(A_{0,R}^-)^2 + (A_{0,I}^-)^2}, \tag{4.17}$$

where $A^-_{0,k} = \int_{-\infty}^{0} g_k(\xi)\,\mathrm{d}\xi$ and $A^-_{1,k} = \int_{-\infty}^{0} \xi\, g_k(\xi)\,\mathrm{d}\xi$, $k = R, I$. Consequently, the scaling exponent α for this class of flows is given by

$$\alpha = \tfrac{1}{3}. \tag{4.18}$$

The numerical confirmation of (4.18) is depicted in figure 6(*b*) for the model flow (4.14). The analysis developed above applies straightforwardly to the class of Couette flows (planar Couette flow, flow between concentric cylinders). The planar Couette flow is defined on a circular strip $\mathscr{M} = \{(x, y) \mid 0 < x < 1, 0 \leqslant y \leqslant 1\}$, where periodicity applies solely to the y-coordinate. Consequently, the boundary conditions for the scalar field $\phi(\boldsymbol{x}, t)$ solution of (1.1) are: periodic boundary condition on the y-coordinate, $\phi(x, 0, t) = \phi(x, 1, t)$, $\partial\phi(x, y, t)/\partial y|_{y=0} = \partial\phi(x, 0, t)/\partial y|_{y=1}$, and zero-flux conditions at $x = 0, 1$, i.e. $\partial\phi(x, y, t)/\partial x|_{x=0} = \partial\phi(x, y, t)/\partial x|_{x=1} = 0$. The velocity field is $\boldsymbol{v}(\boldsymbol{x}) = (0, V(x)/2\pi)$, where $V(x)$ is given by (4.14), and is no longer discontinuous due to the different geometric structure of the flow domain.

The analytic proof of (4.18) for the planar Couette flow is identical to that developed above, and therefore is not repeated here. Figure 6(*b*), line (ii) and dots (•) show the results for the dominant eigenvalue obtained from the direct numerical simulation of (1.1) in the planar Couette case, confirming the $Pe^{-1/3}$ scaling of the convection-enhanced spectral branch. The case of the two-dimensional flow between concentric cylinders (not shown, for the sake of brevity) follows the same scaling, and is discussed in § 6.

5. Quantification of dispersion and homogenization

Section 2 shown the qualitative and phenomenological differences between dispersion in unbounded flows and homogenization in closed bounded domains. This Section attempts a quantitative description of the differences, by comparing the closed-form results obtained for dispersion in unbounded periodic shear flows (Majda & Kramer 1999) with the spectral results derived in § 4.

In order to compare spectral results obtained for closed domains and effective diffusivities in unbounded flows, let us consider a two-dimensional periodic shear model $\boldsymbol{v}_{\mathrm{per}}(\boldsymbol{x})$, defined by the periodization of a simple flow $\boldsymbol{v}(\boldsymbol{x})$ defined on the unit square $\mathscr{I}^2$:

$$\boldsymbol{v}_{\mathrm{per}}(\boldsymbol{x} + n\boldsymbol{e}_1 + m\boldsymbol{e}_2) = \boldsymbol{v}(\boldsymbol{x}), \qquad n, m \text{ integers}, \qquad \boldsymbol{x} \in \mathscr{I}^2, \tag{5.1}$$

where $\boldsymbol{e}_1 = (1, 0)$, $\boldsymbol{e}_2 = (0, 1)$, and $\boldsymbol{v}(\boldsymbol{x}) = (0, v(x))$. Next, we compare this situation with that associated with the advection–diffusion operator defined in $\mathscr{I}^2$, with periodic boundary conditions (which is therefore a flow on a closed and bounded manifold).

In the unbounded case, the dispersion properties are fully characterized by the effective diffusivity tensor $\mathscr{D}^*$ expressed by

$$\mathscr{D}^* = \frac{1}{Pe}\begin{pmatrix} 1 & 0 \\ 0 & 1 + D_y^{(e)} \end{pmatrix}, \tag{5.2}$$

where

$$D_y^{(e)} = Pe^2 \sum_{k=1}^{\infty} \frac{|\widehat{v}_k|^2}{2\pi^2 k^2}, \tag{5.3}$$

and $\widehat{v}_k$ are the Fourier coefficients of the velocity field $v(x) = \sum_{k\neq 0} \widehat{v}_k \mathrm{e}^{2\pi \mathrm{i} k x}$ (Gupta & Bhattacharya 1986; Majda & Kramer 1999). Equation (5.3) differs from the

corresponding equation reported in Majda & Kramer (1999) by a factor $1/Pe$, due to the different dimensionless formulation of the ADE.

Equation (5.3) implies that the sine-flow model $v(x) = \sin(2\pi x)$, and the model flows associated with the potentials $V(x)/2\pi$ defined by (4.13) and by the monotonic potential (4.14) possess the same scaling behaviour in unbounded dispersion, since the two eigenvalues of the effective diffusivity tensor scale proportionally to Pe^{-1} and Pe at large Péclet number, independently of the local details of the flow model.

Conversely, the spectral properties of the advection–diffusion operator defined in $\mathscr{I}^2$ with periodic boundary conditions are altogether qualitatively different in these model flows: $-\mu_R \sim Pe^{-1/2}$ for the sine-flow, $-\mu_R \sim Pe^{-1/3}$ for the tent-map flow (4.13) where $h = 1/4$ and for the flow associated with (4.14), and $-\mu_R \sim Pe^{-1}$ for the flow associated with (4.13) with $h < 1/4$. This result shows unambiguously the profound differences between homogenization in bounded closed flows and dispersion in unbounded domains.

As the effective diffusivity tensor accounts for the possible enhancement effects induced by advection on scalar dispersion, a quantitative parameter serving the same purpose can be introduced for homogenization in bounded closed flows. More specifically, one may define the *diffusion enhancement factor* $E_D(Pe)$ as the ratio between the real part of the dominant eigenvalue belonging to the convection-enhanced branch of the spectrum $-\mu_R(\varepsilon)$ and the dominant diffusive eigenvalue in the absence of advection $-\mu_{\mathrm{dif}}(\varepsilon)$. Since $\mu_{\mathrm{dif}}(\varepsilon) = C_0\varepsilon$, where C_0 is a positive constant depending exclusively on the flow domain, it follows that at large $Pe \geqslant 10^3$

$$E_D(Pe) = \left.\frac{\mu_R(\varepsilon)}{\mu_{\mathrm{dif}}(\varepsilon)}\right|_{\varepsilon = Pe^{-1}} \simeq \frac{K}{C_0} Pe^{1-\alpha}, \tag{5.4}$$

where we have set $-\mu_R(\varepsilon) \simeq K\varepsilon^{\alpha}$, and $K > 0$ is the prefactor. For $\alpha < 1$, the diffusion enhancement factor grows unboundedly as Pe increases with a power law controlled by the exponent $1 - \alpha$. Indeed, the group $1 - \alpha$ can be regarded as an intensive measure of mixing efficiency in closed domains.

6. A kinematic view of universality

It is possible to give a kinematic interpretation of the universality in the scaling of the dominant eigenvalue with respect to the Péclet number. The stretching and folding action of advection determines a progressive shrinking of the lamellar thickness $\delta_{\mathrm{adv}}(t)$ in the absence of diffusion, expressed by the relation $\delta_{\mathrm{adv}}(t) \sim t^{-\zeta}$. In the presence of diffusion, the characteristic diffusive lengthscale is $\delta^2_{\mathrm{dif}}(t) \sim 2\varepsilon t$, and the equilibrium condition between advective stretching and diffusive smoothing is achieved at time t_c defined by the condition

$$\delta_{\mathrm{adv}}(t_c) = \delta_{\mathrm{dif}}(t_c). \tag{6.1}$$

The real part of the dominant exponent $-\mu_R$ corresponds to the reciprocal of the characteristic time t_c, $t_c \simeq (-\mu_R)^{-1}$ at which lamellar shrinking due to advection is compensated by diffusion. By substituting the scaling expressions for these two quantities it follows that

$$(-\mu_R)^{-1} \simeq t_c \sim \varepsilon^{-1/(2\zeta+1)}, \tag{6.2}$$

and comparison of (4.12) and (6.2) yields $\zeta = \gamma^{-1}$, which means that the scaling of the lamellar thickness is inversely proportional to the nonlinearity exponent γ of the flow near its critical point. The validity of this result can be easily checked numerically by means of simple kinematic simulations. In fact, the lamellar thickness $\delta_{\mathrm{adv}}(t)$ can

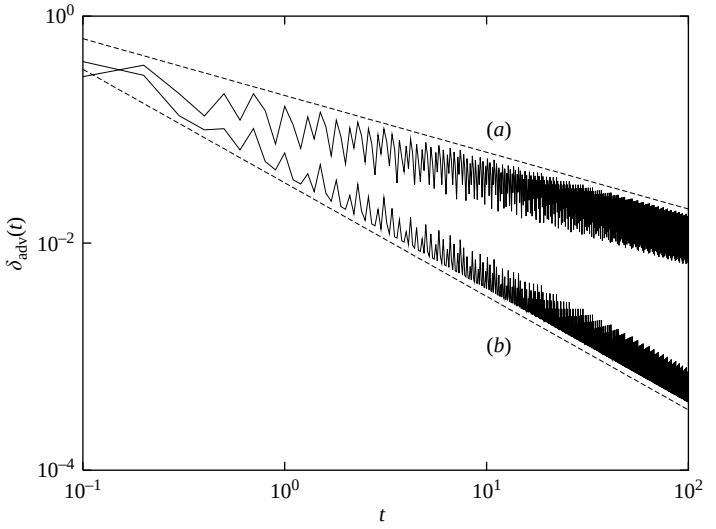

FIGURE 7. $\delta_{\rm adv}(t)$ vs t. (*a*) The sine-flow, and the upper dashed line is $\delta_{\rm adv}(t) \sim t^{-1/2}$ ($\gamma = 2$). (*b*) The model flow driven by the tent potential (4.13) with $h = 1/4$. The lower dashed line is $\delta_{\rm adv}(t) \sim t^{-1}$ ($\gamma = 1$).

be approximatively estimated as follows: consider a material interface $\Gamma(0)$ and a cross-section Σ, both orthogonal to the flow, and let $\Gamma(t)$ be the image of $\Gamma(0)$ at time t resulting from the advection action. Let $\{x_i(t)\}$ be the ordered intersections of $\Gamma(t)$ with Σ at time t, $x_i < x_{i+1}$, and define $\delta_{\rm adv} = \max_i(x_{i+1} - x_i)$. Figure 7 shows the simulation results for the two model flows considered in § 4.2 (in these simulations $\Gamma(0)$ is the line segment $y = 0$, and Σ the segment $y = 1/2$), which agree with the scaling result expressed by $\delta_{\rm adv}(t) \sim t^{-1/\gamma}$.

The analysis of the scaling behaviour of $\delta_{\rm adv}(t)$ provides a simple Lagrangian approach to infer the scaling of the convection-enhanced branch of the ADE spectrum without performing any direct spectral estimates. For example, let us consider the family of Couette flows. Figure 8 shows the scaling of $\delta_{\rm adv}(t)$ for the planar Couette flow (4.14), and for the two-dimensional flow between concentric cylinders (Couette flow *sensu stricto*), defined in the flow domain $\mathscr{M} = \{(r, \theta) \mid R_1 < r < R_2\ 0 \leqslant \theta \leqslant 2\pi\}$, expressed in cylindrical coordinates (r, θ). The dimensionless radii are $R_1 < R_2 = 1$. Kinematic analysis confirms the value $\alpha = 1/3$ for the planar Couette flow, since $\zeta = 1$. The Lagrangian analysis of the flow between concentric cylinders is performed by considering the kinematic equation $\dot{\theta} = v_\theta(r)/r$, where $v_\theta(r) = \Omega r(1 - R_1^2/r^2)/(1 - R_1^2/R_2^2)$, $\Omega = 1$, and an initial segment and the cross-section Σ located at $\theta = 0$, and $\theta = \pi$, respectively. The scaling $\delta_{\rm adv}(t) \sim t^{-1}$ characterizing the kinematic properties independently of R_1 supports the observation that $-\mu_R(\varepsilon) \sim \varepsilon^{1/3}$ for this class of flows.

7. Concluding remarks

Equation (3.5) is the simplest one-dimensional model, not based on any approximation (such as the lamellar models, see Ottino 1989), which explains the basic features of dispersion in two-dimensional autonomous bounded flows. Dispersion regimes that show a real coupling between advection and diffusion (i.e. a scaling exponent $\alpha < 1$) are characterized by eigenfunction localization and by the presence of a boundary

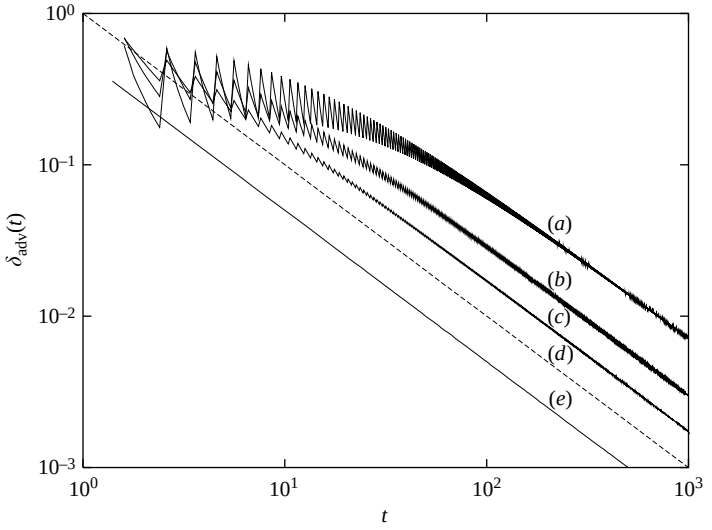

FIGURE 8. $\delta_{adv}(t)$ vs t for the Couette flow. (*a–c*) Inner cylinder radius R_1 equal to 0.3, 0.5, 0.7, respectively. Dashed line (*d*) is the scaling $\delta_{adv}(t) \sim t^{-1}$. (*e*) The planar Couette flow (4.14).

layer, the width of which scales as $\beta(\varepsilon) \sim \varepsilon^{1/(2\gamma+1)}$. The scaling behaviour (4.12) for $\gamma \to \infty$ has a simple fluid dynamic explanation: whenever there exist finite domains in which the deformation tensor identically vanishes (possibly present in a Bingham fluid flow), a diffusive scaling in homogenization kinetics occurs. Spectral analysis of bounded flows provides the most intuitive and natural quantification of mixing in the presence of diffusion, since the real parts of the dominant eigenvalues of the different spectral branches are inversely proportional to the characteristic homogenization times.

Universality in the advection–diffusion equation (which has some analogies with the Feigenbaum universality for unimodal maps) has been proved by means of functional arguments, but has a simple explanation based on purely kinematic properties (as briefly outlined in § 6). The universal features characterizing the simple class of flows considered in this article explain the phenomenology observed numerically for several two-dimensional autonomous closed flows (e.g. the driven cavity flow), namely the occurrence of an eigenvalue branch that scales as $Pe^{-1/2}$. Very succintly, this can be argued as follows. If one expresses the ADE in a streamfunction-based orthogonal system, the velocity field has only one non-vanishing component (since it is tangent to the streamlines), analogously to the simple model flows considered in this article. Since it is a generic property for smooth velocity fields that this non-vanishing entry has a local behaviour near its critical points which is quadratic (i.e. $\gamma = 2$), the scaling $-\mu_R \sim Pe^{-1/2}$ follows. While the $Pe^{-1/2}$-scaling is generic for autonomous two-dimensional flows with a local maximum/minimum of the velocity in a stream-based orthogonal system, there are significant exceptions to it, as the case of the Couette flow demonstrates, for which $-\mu_R \sim Pe^{-1/3}$.

To summarize, the spectral analysis developed in this article provides a complete understanding of homogenization dynamics in closed and bounded two-dimensional autonomous flows. Further developments of the theory should be oriented toward the understanding of spectral properties of the ADE in two-dimensional partially chaotic flows, which display eigenfunction localization properties around the region of poor

kinematic mixing (quasi-periodic regions), and consider values of the exponent α controlling the scaling of the dominant eigenvalue between 0 and 1 (Giona *et al.* 2004).

REFERENCES

Agmon, S. 1962 On the eigenfunctions and on the eigenvalues of general elliptic boundary value problems. *Commun. Pure Appl. Maths* **15**, 119–147.

Agmon, S. 1965 *Lectures on Elliptic Boundary Value Problems*. Van Nostrand.

Batchelor, G. K. 1956 On steady laminar flow with closed streamlines at large Reynolds number. *J. Fluid Mech.* **1**, 177–190.

Bensoussan, A., Lions, J.-L. & Papanicolau, G. 1978 *Asymptotic Analysis for Periodic Structures*. North-Holland.

Castiglione, P., Mazzino, A., Muratore-Gianneschi, P. & Vulpiani, A. 1999 On strong anomalous diffusion. *Physica* D **134**, 75–93.

Cerbelli, S., Adrover, A. & Giona, M. 2003 Enhanced diffusion regimes in bounded chaotic flows. *Phys. Lett*. A **312**, 355–362.

Childress, S. & Soward, A. M. 1989 Scalar transport and alpha-effect for a family of cat's-eye flows. *J. Fluid Mech.* **205**, 99–133.

Fannjiang, A. & Papanicolau, G. 1994 Convection enhanced diffusion for periodic flows. *SIAM J. Appl. Maths* **54**, 333–408.

Feigenbaum, M. J. 1979 The universal metric properties of nonlinear transformations. *J. Statist. Phys.* **21**, 669–706.

Giona, M. & Adrover, A. 1998 Nonuniform stationary measure of the invariant unstable foliation in hamiltonian and fluid mixing systems. *Phys. Rev. Lett*. **81**, 3864–3867.

Giona, M., Adrover, A., Cerbelli, S. & Vitacolonna, V. 2004 Spectral properties and transport mechanisms of partially chaotic bounded flows in the presence of diffusion. *Phys. Rev. Lett*., **92**, 114101.

Giona, M., Cerbelli, S. & Adrover, A. 2002 Quantitative analysis of mixing structures in chaotic flows generated by infinitely fast reaction in the presence of diffusion. *J. Phys. Chem.* **106**, 5722–5736.

Goldsheid, I. Ya. & Khoruzhenko, B. A. 2000 Eigenvalue curves of asymmetric tridiagonal random matrices. *Electronic J. Prob.* **5**, 1–28.

Gupta, V. K. & Bhattacharya, R. N. 1986 Solute dispersion in multidimensional periodic saturated porous media. *Water. Resour. Res.* **22**, 156–164.

Hatano, N. & Nelson, D. R. 1996 Localization Transition in non-hermitian quantum mechanics. *Phys. Rev. Lett*. **77**, 570–573.

Holmes, M. H. 1995 *Introduction to Perturbation Methods*. Springer-Verlag.

Liu, M., Muzzio, F. J. & Peskin, R. L. 1994 Quantification of mixing in aperiodic flow. *Chaos, Solitons and Fractals* **4**, 869–893.

Majda, A. J. & Kramer, P. R. 1999 Simplified models for turbulent diffusion: Theory, numerical modelling and physical phenomena. *Phys. Rep.* **314**, 237–574.

Ottino, J. M. 1989 *The Kinematics of Mixing – Stretching, Chaos, and Transport*. Cambridge University Press.

Toussaint, V., Carriere, P. & Raynal, F. 1995 A numerical Eulerian approach to mixing by chaotic advection. *Phys. Fluids* **7**, 2587–2600.

Toussaint, V., Carriere, P., Scott, J. & Gence, J.-N. 2000 Spectral decay of a passive scalar in chaotic mixing. *Phys. Fluids* **12**, 2834–2844.